Title
Characteristic performance evaluation of a photon counting Si strip detector for low dose spectral breast CT imaging

Journal
Medical Physics, 41(9)

ISSN
0094-2405

Authors
Cho, Hyo-Min
Barber, William C
Ding, Huanjun
et al.

Publication Date
2014-08-13

DOI
10.1118/1.4892174

Characteristic performance evaluation of a photon counting Si strip detector for low dose spectral breast CT imaging

Hyo-Min Cho
Department of Radiological Sciences, University of California, Irvine, California 92697

William C. Barber
DxRay Inc., Northridge, California 91324

Huanjun Ding
Department of Radiological Sciences, University of California, Irvine, California 92697

Jan S. Iwanczyk
DxRay Inc., Northridge, California 91324

Sabee Molloi[a)]
Department of Radiological Sciences, University of California, Irvine, California 92697

(Received 14 January 2014; revised 16 July 2014; accepted for publication 19 July 2014; published 13 August 2014)

Purpose: The possible clinical applications which can be performed using a newly developed detector depend on the detector's characteristic performance in a number of metrics including the dynamic range, resolution, uniformity, and stability. The authors have evaluated a prototype energy resolved fast photon counting x-ray detector based on a silicon (Si) strip sensor used in an edge-on geometry with an application specific integrated circuit to record the number of x-rays and their energies at high flux and fast frame rates. The investigated detector was integrated with a dedicated breast spectral computed tomography (CT) system to make use of the detector's high spatial and energy resolution and low noise performance under conditions suitable for clinical breast imaging. The aim of this article is to investigate the intrinsic characteristics of the detector, in terms of maximum output count rate, spatial and energy resolution, and noise performance of the imaging system.

Methods: The maximum output count rate was obtained with a 50 W x-ray tube with a maximum continuous output of 50 kVp at 1.0 mA. A ^{109}Cd source, with a characteristic x-ray peak at 22 keV from Ag, was used to measure the energy resolution of the detector. The axial plane modulation transfer function (MTF) was measured using a 67 μm diameter tungsten wire. The two-dimensional (2D) noise power spectrum (NPS) was measured using flat field images and noise equivalent quanta (NEQ) were calculated using the MTF and NPS results. The image quality parameters were studied as a function of various radiation doses and reconstruction filters. The one-dimensional (1D) NPS was used to investigate the effect of electronic noise elimination by varying the minimum energy threshold.

Results: A maximum output count rate of 100 million counts per second per square millimeter (cps/mm^2) has been obtained (1 million cps per 100 $\times$ 100 μm pixel). The electrical noise floor was less than 4 keV. The energy resolution measured with the 22 keV photons from a ^{109}Cd source was less than 9%. A reduction of image noise was shown in all the spatial frequencies in 1D NPS as a result of the elimination of the electronic noise. The spatial resolution was measured just above 5 line pairs per mm (lp/mm) where 10% of MTF corresponded to 5.4 mm^{-1}. The 2D NPS and NEQ shows a low noise floor and a linear dependence on dose. The reconstruction filter choice affected both of the MTF and NPS results, but had a weak effect on the NEQ.

Conclusions: The prototype energy resolved photon counting Si strip detector can offer superior imaging performance for dedicated breast CT as compared to a conventional energy-integrating detector due to its high output count rate, high spatial and energy resolution, and low noise characteristics, which are essential characteristics for spectral breast CT imaging. [http://dx.doi.org/10.1118/1.4892174]

Key words: photon counting detector, Si strip, spectral breast CT, characteristic evaluation

1. INTRODUCTION

Breast cancer is one of the most frequently diagnosed cancers among women in the US.[1] Clinically used breast imaging technologies include mammography, digital breast tomosynthesis (DBT),[2,3] magnetic resonance imaging (MRI),[4,5] and breast ultrasound.[6] However, each of these modalities has its own limitations in breast cancer diagnosis. Dedicated cone beam breast computed tomography (CT) based on energy-integrating flat panel detectors, which scans in the coronal

plane around the breast in its pendant geometry, has been recently investigated to address some of the limitations of the current breast imaging techniques.[7,8] Initial clinical studies have shown that flat panel based breast CT images are significantly better than screen-film mammograms for visualization of soft tissue masses.[9] However, micro-calcifications detection, which is an important signature of breast cancer, is one of the major limitations of the flat panel based breast CT systems.[8,10]

The limitations of flat panel based systems can be potentially addressed with the recent development of energy resolved photon counting x-ray detectors. These detectors outperform conventional energy-integrating flat panel detectors at a low dose level due to three main advantages.[11] First, the electronic noise caused by the detector does not contribute to the image like it would with conventional energy integrating flat panel detectors. A proper noise floor can be selected by changing the lowest energy threshold in order to reject the electronic noise. Second, the suboptimal energy response function of conventional energy-integrating flat panel detectors, which places a weight on each x-ray proportional to its energy, is eliminated thus increasing the contrast to noise ratio (CNR). The CNR can be further improved by using optimal energy weighting, which generally increases the contribution of the low energy photons, since the difference in attenuation coefficients for different tissue types decreases as a function of energy. Third, multiple energy windowed images that are acquired simultaneously with minimum spectral overlap can be used for quantitative material identification. An ideal breast imaging technique should offer high contrast and spatial resolution, to detect both soft tissue lesion and micro-calcifications in three-dimensional (3D) imaging with an average dose equal or less than 6 mGy.[12] The combination of breast CT and energy resolved photon counting detectors could offer the possibility of a spectral breast CT system capable of soft tissue lesion and microcalcification detection at low dose.[11,12]

Most of the energy resolved photon counting detectors developed for high flux x-ray imaging are based on direct conversion semiconductor sensors, such as silicon (Si),[13] Cadmium Telluride (CdTe),[14] and Cadmium-Zinc-Telluride (CZT).[11,15,16] CdTe and CZT have high x-ray stopping power owing to their high atomic number. However, in the case of small 100 μm pixels, which are essential for microcalcifications detection in breast imaging, CdTe and CZT can suffer from charge sharing at energies above the K-edge of Cd and Te when the fluorescence x-rays are detected by neighboring pixels by reabsorption, thus, distorting the spatial and energy resolution. In contrast, Si is free of charge sharing from fluorescence escape. In addition, Si has a much higher charge carrier mobility than CdTe/CZT.[17] Charge sharing between pixels due to the coulomb diffusion of electrons in the primary charge cloud is minimal due to the small thickness of the Si junction (0.5 mm) and the high charge carrier mobility. While the quantum detection efficiency (QDE) of Si strip detectors declines as the x-ray tube voltage increases due to its relatively low atomic number, it can still offer good detection efficiency for breast imaging if edge-on illumination is used.[18] This is due to the fact that optimized spectra for dedicated breast CT imaging are expected to be in the range of 40 to 70 kVp.[19] In this study, a prototype photon counting detector, which consists of Si strips in edge-on geometry with fast readout electronics, was investigated for the application of spectral breast CT imaging.

The high count rates obtained are related to the rapid charge collection across the narrow 0.5 mm junction of the Si detector and the corresponding fast electronics. The maximum count rate is limited by pulse pileup.[20] Energy resolution is an important characteristic of energy resolved photon counting detectors and is related to the charge collection efficiency and the electronic noise. A narrow width of the pulse height distribution from a monoenergetic source is indicative of good energy resolution of the detector. The distribution of the pulse heights reflects the fluctuation from pulse to pulse when the same energy photon is deposited for many events.[21] The modulation transfer function (MTF), the noise power spectrum (NPS), and the noise equivalent quanta (NEQ) have been used as physical factors that govern multidimensional imaging performance.[22] The spatial frequency dependent signal and noise transfer characteristics can be understood from these three parameters.

The purpose of this study was to evaluate the performance of a novel energy resolved photon counting Si strip detector for its potential application in a dedicated spectral breast CT system. The study characterized the prototype Si strip detector in terms of its maximum output count rate, energy resolution, 2D spatial resolution using MTF, and the noise performance by calculating the NPS, and the NEQ in reconstructed images at various doses and with different reconstruction filters.

2. MATERIALS AND METHOD

2.A. Intrinsic characteristics of the detector

2.A.1. Photon counting Si strip detector

Figure 1(a) shows a schematic of a side view of the investigated Si strip detector. The detector consisted of a single line of 256 pixels with a pixel pitch of 100 μm. The Si sensor is 0.5 mm thick and 1.0 cm long. Edge illumination was designed with a 5° angle tilt, which created 0.6 cm effective attenuation for the incident x-rays. One advantage to this design is that the edge illumination provides a small charge transport time (the charge must only travel 0.5 mm across the junction) which allows for the rapid signal formation required of the fast application specific integrated circuit (ASIC) design to produce a high output count rate.

2.A.2. ASIC readout electronics

Figure 1(b) shows a schematic of the ASIC used in this detector. The ASIC contains charge-sensitive preamplifiers, shaping amplifiers, four energy level threshold discriminators per preamplifier, and digital event counters which are available for each threshold discriminator in the ASIC. The threshold levels of all discriminators can individually be fine-tuned through separate 6-bit digital to analog converters (DACs)

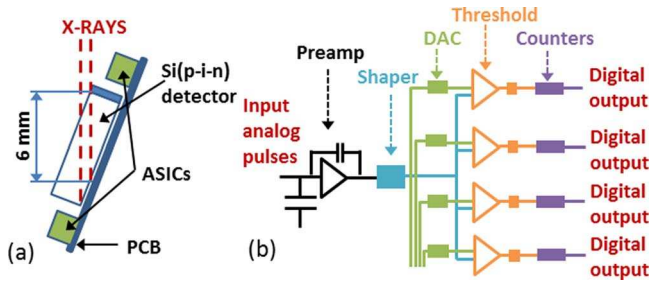

FIG. 1. Schematic of (a) the edge illuminated Si strip detector and (b) the ASICs.

attached to each discriminator. These four threshold levels are externally adjustable. When photons strike the detector crystals, the generated electrons and holes will propagate toward the electrodes in opposite directions due to the applied electric field. These electrical charges produce a pulse signal that is amplified and the height of the pulse is compared to user selectable thresholds. A corresponding counter increases a count if the pulse height exceeds a threshold value. Four comparators sort the photons into four energy windows. The total photon count in each energy window is obtained by subtracting counts in counters from adjacent energy thresholds.

2.A.3. Energy calibration

An energy calibration was performed by two methods. First a 50 W x-ray tube with a focal spot size of 0.25 mm (CMX005, Source 1 X-Ray, Campell, CA) was calibrated using a high detection efficiency energy dispersive CdTe detector previously calibrated with ^{109}Cd, ^{133}Ba, and ^{241}Am sources after which the calibrated max kVp setting on the tube was adjusted from 13 to 50 kVp and the x-rays with the highest energy recorded by the Si strip detector were assumed to have an energy equal to the max kVp setting on the tube. Second, spectra from 9.229 μCi ^{109}Cd and 8.744 Ci ^{133}Ba sources were acquired for several minutes with the Si strip detector to verify the first calibration.

2.A.4. Count rate performance

The output count rate as a function of input count rate has been measured by setting one threshold just above the electronic noise floor and recording all the counts with energy above the threshold setting as a function of time. A 50 W x-ray tube (CMX005, Source 1 X-Ray, Campell, CA) was set to 50 kVp and the tube current was increased from 1 μA to 600 μA with a thick 0.1 mm wide slit collimator 1 cm above the detector. This collimator geometry creates a 1D row of 100 $\times$ 100 μm pixels. A 0.5 mm thick Cu filter was used with a source to detector distance of roughly 20 cm.

2.A.5. Energy resolution

The energy resolution was measured by using characteristic x-ray peak of Ag at 22 keV which was produced by the decay of a ^{109}Cd source. A 9.229 μCi ^{109}Cd source was placed on a thick 0.5 mm wide slit brass collimator 1 cm above the detector. This collimator geometry creates a 1D row of 100 $\times$ 500 μm pixels with a 100 μm pitch along the long axis. The counts above a single threshold set to 100 keV are recorded during a fixed frame time and then the threshold's setting is lowered by 0.25 keV and the exposure is repeated covering a range from 100 to 0 keV. The function of the number of counts above the threshold setting is digitally differentiated by a forward-backwards method to a pole of order 5 to generate the spectrum. The photo peak at 22 keV fitted to a Gaussian function whose full width at half maximum (FWHM) is used to determine the energy resolution.

2.A.6. Pixel sensitivity variation

The pixel sensitivity variation was investigated by acquiring an open flood field image under linear output count rate response condition. The image was acquired at 65 kVp, 2.5 mA with a frame time of 50 ms. A flat-field correction technique using separately acquired open flood field image was implemented to compensate for the sensitivity variation across pixels. The efficiency of the flat-field correction was evaluated using the image uniformity factor which was calculated using the maximum (C_{max}) and minimum (C_{min}) counts in the entire image. The uniformity (U) is calculated using

$$U = \left[1 - \frac{(C_{max} - C_{min})}{(C_{max} + C_{min})}\right]. \quad (1)$$

2.B. Imaging performance of the detector in a spectral CT system

2.B.1. Spectral CT imaging system

The experiments were conducted using a bench-top CT system, which consisted of a tungsten target 160 W x-ray tube (XRB101, Spellman, Hauppauge, NY) with a maximum continuous output of 150 kVp at 4 mA and the energy resolved photon counting Si strip line detector. Fore- and aft-collimators were used to create fan beam geometry. The slice thickness, determined by the aft-collimator, was 0.5 mm. Figure 2 depicts a schematic of the experimental setup. Due to the limitations from the x-ray tube focal spot size (0.8 mm) and the detector's field of view (FOV), the source-to-object distance (SOD) and the source-to-detector distance (SDD) of the system was set to be 96 and 105 cm, respectively. This led to a system magnification of approximately 1.1.

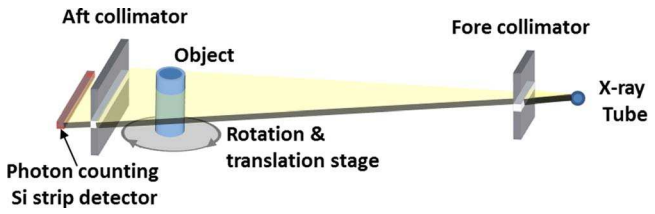

FIG. 2. Schematic of the experimental setup.

2.B.2. Acquisition parameters

The tube voltage was set at 65 kVp with 2.7 mm Al filtration and a half value layer (HVL) of 2.18 mm Al which matched a dose efficient optimal spectrum for dedicated breast CT.[12,19] Different dose levels were used by adjusting the tube current (mA), with considering both the detector's output count rates and tube power. The phantoms were rotated by 360° and a total of 863 projections were acquired per rotation. The photon counting integration time per frame was 50 ms, yielding an effective frame rate of 20 frames/s. The dose level to the detector was measured as the air kerma (mGy) using a calibrated ionization chamber (20 × 6-0.6, Radcal, Monrovia,CA) with no backscatter from the detector. The exposure was determined from an average of five exposure measurements at the isocenter. The resulting air kerma at the isocenter was 3 mGy per CT scan with a tube current setting of 2.5 mA.

Various doses and reconstruction filters were used to investigate their effect on the imaging performance. The dose was modified to 1.5, 3, and 6 mGy air kerma per scan. A filtered backprojection (FBP) method was used for the image reconstruction. The application of a smoothing filter is a common method to reduce or remove high-frequency noise amplified by the ramp filter.[23] The effect of the reconstruction filter was studied by reconstructing data with various smoothing filters, such as Shepp-Logan, Cosine, Hamming, and Hanning filters at the same dose level.

2.B.3. Modulation transfer function

The axial plane MTF was measured using a tungsten wire of 67 μm in diameter. The tungsten wire was placed 2 mm away from the isocenter.[12,24] 863 projections were acquired for a scan time of 43 s and reconstructed in 512 × 512 matrix size using a FBP with a ramp filter. The reconstructed pixel size was 0.045 mm. The line spread functions (LSF) of the wire were acquired in a region of interest (ROI) of 100 × 100 pixels near the wire. The center of LSF was determined by calculating the centroid of the selected ROI and then the LSF were averaged over 180° with respect to the center. The MTF was calculated by taking the one-dimensional fast Fourier transform of the LSF.

2.B.4. Noise power spectrum

Electronic noise can produce undesirable fluctuations in the signal and it is present at certain levels in any electrical measurement. In energy-integrating detectors, an individual pixel's variance can include electronic noise and Swank noise.[15] With the investigated photon counting detector, these noise sources, however, can be eliminated without any loss of signal by setting the lowest threshold above the noise floor.[25] Since the NPS is a measure of noise power, the integral over all frequencies of the NPS will yield the pixel variance of the noise data.[26] Overall noise level in the open field image is determined by the incident photon flux and the electronic noise which is caused by the electronics in the detector. Therefore, the elimination of electronic noise can be investigated using NPS.[15,27] Dark field images were acquired with various lowest threshold levels from 0 to 10 keV to find the optimal threshold to maximize the elimination of electronic noise. Five independent measurements at each threshold were performed.

The NPS with different dimensions can be used to evaluate noise properties of the system with different purposes even though they are closely related. The 1D normalized NPS (NNPS) and 2D NPS were calculated with and without electronic noise to investigate spatial frequency dependent noise reduction. The reconstructed image quality for different doses and reconstruction filters was also evaluated using the 2D NPS. Since the detector has one line of pixels, all pixels' data were used to calculate 1D NNPS. The four projection images were averaged and then subtracted from one of the images to remove the background trends. The Fourier transform was applied and normalized with the square of the mean signal used for analysis. The 1D NNPS curves were generated with the exclusion of the center axis data.[28] To calculate the 2D NPS, the projection images were reconstructed in matrix size of 512 × 512 with pixel size of 0.045 mm using FBP. The reconstructed matrix and pixel sizes were properly selected to avoid noise aliasing in the frequency domain.[29] The difference image between two identical scans was used for all the 2D NPS calculations to eliminate structured noise. The doubling of noise power due to the subtraction was compensated in the NPS calculation.[29,30] The reconstructed images where the pixel values have a zero-mean were separated into four half-overlapped 220 × 220 sub ROIs. The 2D NPS is defined as

$$\mathrm{NPS}(u,v) = \frac{1}{M}\sum_{i=1}^{M}\frac{\left|FFT_{2D}[I_i(x,y)-\bar{I}_l]\right|^2}{2}\frac{\Delta x\,\Delta y}{N_x N_y}, \tag{2}$$

where $I_i(x, y)$ is the ith sub ROI from reconstructed noise image; $\bar{I}_l$ is the mean value of corresponding sub ROI; u and v are the spatial frequencies conjugate to x and y, respectively; $N_x = 220$ and $N_y = 220$ are the numbers of elements in x and y directions, respectively; Δx and Δy are the corresponding pixel sizes in each direction; and M is the total number of ROIs.[23,29]

2.B.5. Noise equivalent quanta

The NEQ is a figure of merit for imaging performance which describes the spatial-frequency dependence on the effective number of photons, quantifies the tradeoffs between spatial resolution and noise.[22] The 2D NEQ was calculated according to

$$\mathrm{NEQ}(u,v) = \theta_{tot} f \frac{MTF^2(u,v)}{NPS(u,v)}, \tag{3}$$

where θ_{tot} is the total acquisition angle of scan and f is the sampling frequency.

3. RESULT

3.A. Intrinsic characteristics of the detector

3.A.1. Energy calibration

Figure 3 shows the energy calibration curve for a typical 100 μm pixel of the Si strip detector acquired with a calibrated x-ray tube by using the max kVp method described in Sec. 2. Tube voltages of 13, 15, 22, 30, 40, and 50 kVp were used. A linear fit to the response is used to initially calibrate the detector; and radionuclide sources are used to verify the calibration. Extrapolation of the line to 0 keV indicates that the preamplifier offset is approximately 30 mV.

3.A.2. Count rate performance

Figure 4 shows the output count rate as a function of tube current which is proportional to the input count rate, for a typical 100 μm pixel of the Si strip detector. The output is linear to 40 Mcps/mm^2 and saturates just below 100 Mcps/mm^2.

3.A.3. Energy resolution

Figure 5 shows a ^{109}Cd spectrum as a function of energy for a typical 100 μm pixel of the Si strip detector. The FWHM energy resolution is approximately 1.7 keV or 8.5% at 22 keV.

3.A.4. Pixel sensitivity variation

Figure 6 shows the profiles before and after flat-field correction. The counts gradually reduced from the 1st pixel to the 256th pixel before flat-field correction. The pixel variation was significantly reduced after applying the flat-field correction. The uniformity factor was improved from 0.79 to 0.93.

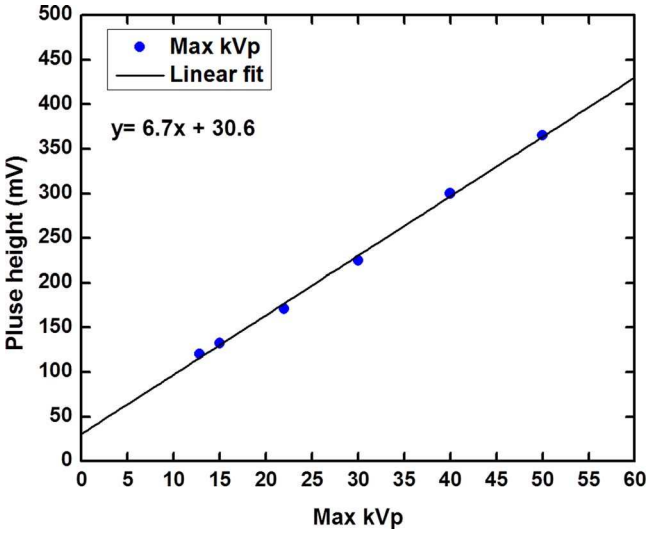

FIG. 3. Graph of the detector pulse height as a function of the maximum photon energy.

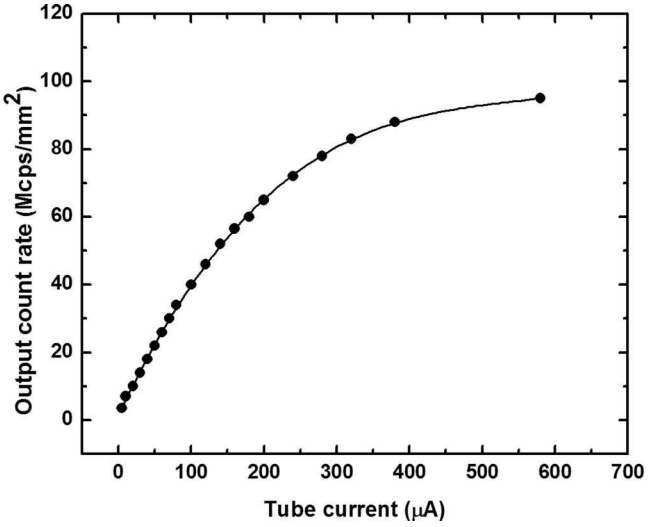

FIG. 4. Graph of the output count rate as a function of x-ray tube current.

3.B. Imaging performance of the detector in a spectral CT system

3.B.1. Electronic noise

Figure 7(a) shows the mean pixel values of the dark field images acquired with different lowest threshold settings ranging from 0 to 6 keV. Error bars show the standard deviations of five independent measurements. The mean pixel values decreased monotonically as lowest threshold increased and became essentially zero after 4 keV, which was determined to be the lowest threshold for electronic noise rejection. Figure 7(b) shows the 1D NNPS acquired with a lowest threshold of 0 and 4 keV, which corresponded to the presence and absence of the electronic noise, respectively. The noise reduction is clearly shown through the entire spatial frequency range. Figure 7(c) shows the 2D NPS results with and without electronic noise. The noise reduction is clearly displayed especially at low

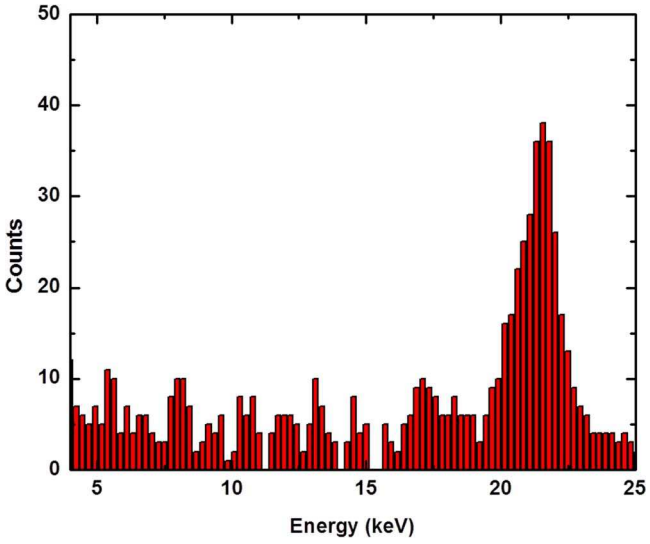

FIG. 5. Graph of differentiated energy calibrated S-curves for a ^{109}Cd source.

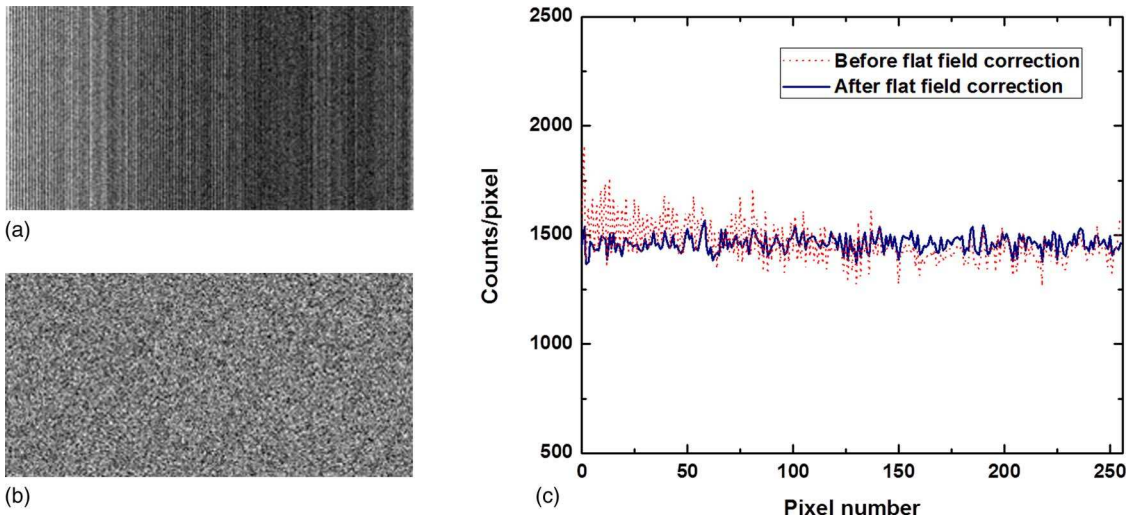

FIG. 6. Open field images of (a) before and (b) after flat-field correction. (c) Profiles of acquired open field image before and after flat-field correction.

spatial frequency where the electronic noise contributes more to the image noise.

3.B.2. 2D MTF, NPS, NEQ with various doses

The axial plane MTF at 3 mGy is shown in Fig. 8(a). The 10% of MTF value was determined to be 5.4 mm^{-1} which indicated that the minimum detectable size of an object with sufficient contrast to the background is expected to be approximately 93 μm. This value is in agreement with the expectation from our detector pixel size and system magnification settings. The measured 2D NPS for three different levels of dose are shown in Fig. 8(b) in the axial domain. The results showed that the noise power decreased linearly with an increase of the dose while the NPS curve trends in terms of shape are very similar which are affected in part by the reconstruction filter. The linear dependence of NEQ on dose can be expected when we consider that NEQ is calculated by dividing MTF by the NPS according to Eq. (2). Figure 8(c) also shows that the axial plane NEQ increased proportionally with respect to the radiation dose.

3.B.3. 2D MTF, NPS, NEQ with various reconstruction filters

Figure 9 shows the MTF, NPS, and NEQ results with various reconstruction filters which are commonly used with FBP. The smoothing degree increases in the following order of the filters: Ramp, Shepp-Logan, Cosine, Hamming, and Hanning. Figure 9(a) demonstrates the spatial resolution reduction according to the smoothing filter as well as the noise reduction in axial NPS plot in Fig. 9(b). The spatial resolution degradation and reduction of noise as compared with the ramp filter were dependent on each filter and cutoff frequency. Since NEQ is calculated by the ratio of spatial resolution and noise, the NEQ results show only a weak dependence on the reconstruction filter.

4. DISCUSSION

The prototype Si-based energy resolved photon counting detector was investigated in terms of an intrinsic characterization: by measuring the maximum output count rate, energy resolution, and pixel sensitivity variation. Imaging performance was evaluated in the fan beam CT system using 2D MTF, NPS, and NEQ.

In order to take advantage of the spectral information from an energy resolved photon counting detector, the detector needs to be calibrated for its energy response. Based on the linear result shown in Fig. 3, the threshold values in pulse height (mV) can be converted to energy (keV) using the slope (gain) and intercept (offset) of a linear fit applied to the energy response curve. The main uncertainty in energy calibration comes from the threshold levels in the ASIC, which are able to be set with an accuracy of ± 0.5 keV due to variance in the voltage setting of the comparators. Inaccuracies in the voltage setting of the x-ray tube or the determination of the recorded x-rays with the highest energy are generally smaller. A more accurate calibration method using radionuclide sources may slightly improve the calibration. However, this method is very time consuming given the small pixel size. In this study, we did not observe significant differences between the two calibration methods.

The maximum output count rate of 100 Mcps/mm^2 shown in Fig. 4 is high enough for breast CT applications when we consider the average true count rates between 1 and 10 Mcps/mm^2.[31] The required detector count rate can be estimated using the number of projections as 863, frame time of 50 ms, magnification factor of 1.1, detector pixel size of 0.5 $\times$ 0.1 mm^2, and input photon flux of 163 781 photons/mR/mm^2. The true count rate was calculated to be 0.5, 1, and 2 Mcps/mm^2 for total exposures of 1.5, 3, and 6 mGy, respectively. Attenuation by the object was not considered, which will further reduce the required count rate.

Figure 5 shows the excellent energy resolution of the photon counting detector. Although the flux from the source is significantly less than standard imaging procedures, the same

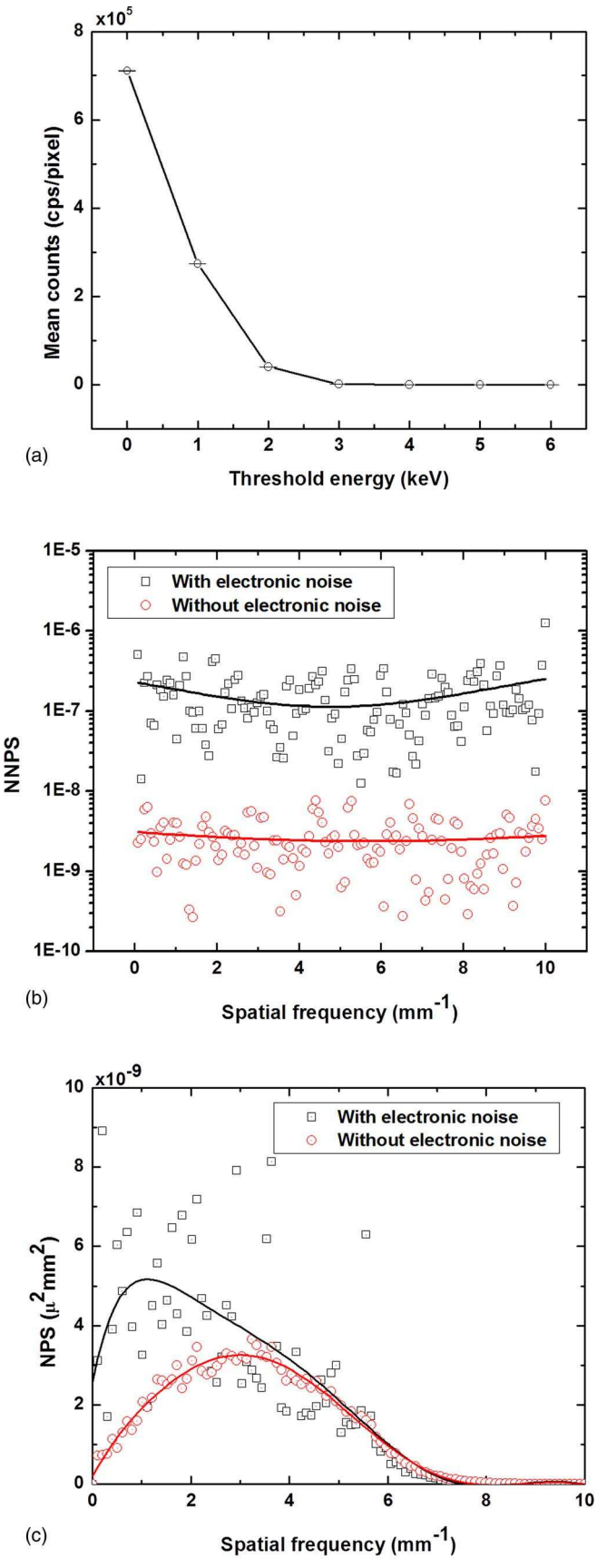

FIG. 7. (a) Mean counts of each pixel at dark field image as a function of the lowest energy threshold from 0 to 10 keV. (b) The 1D NNPS with and without electronic noise and (c) the 2D NPS with and without electronic noise at 65 kVp and 3 mGy. Polynomial fits were applied.

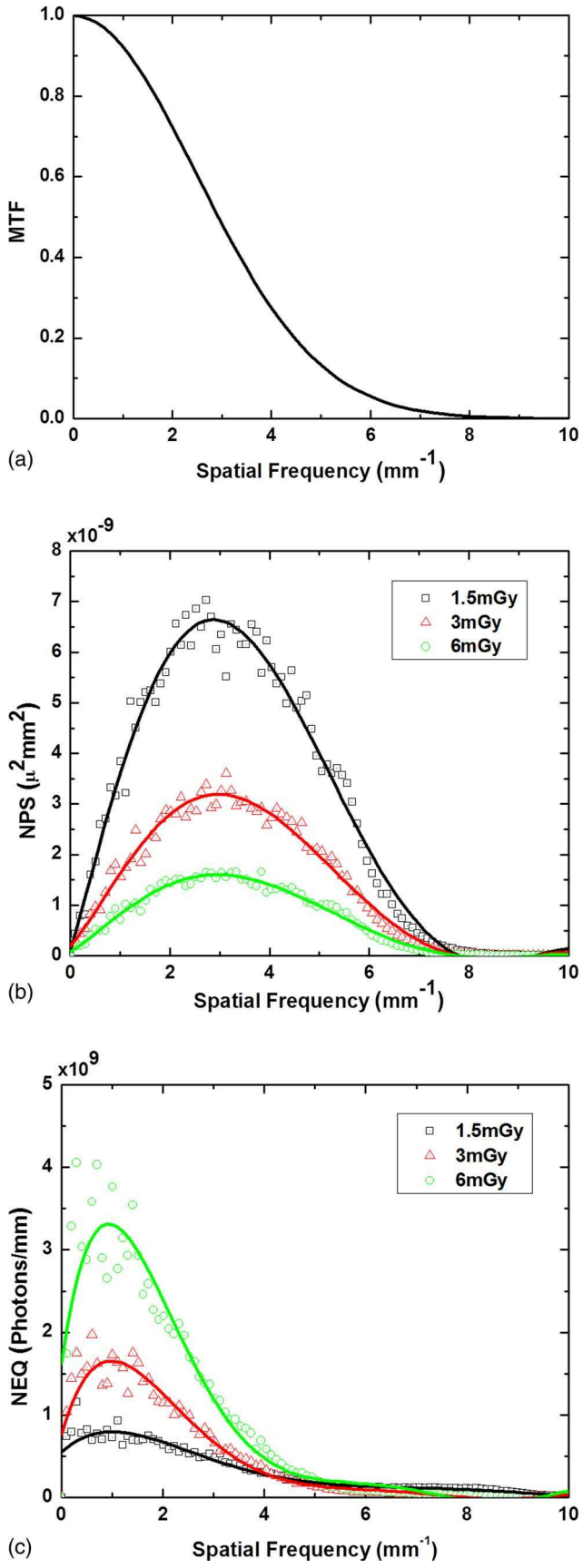

FIG. 8. (a) The axial MTF as a function of spatial frequency at 3 mGy. The 2D (b) NPS and (c) NEQ were acquired as a function of spatial frequency at three different doses. The solid line represents the polynomial fits to the data points. All results calculated from images reconstructed with ramp filter.

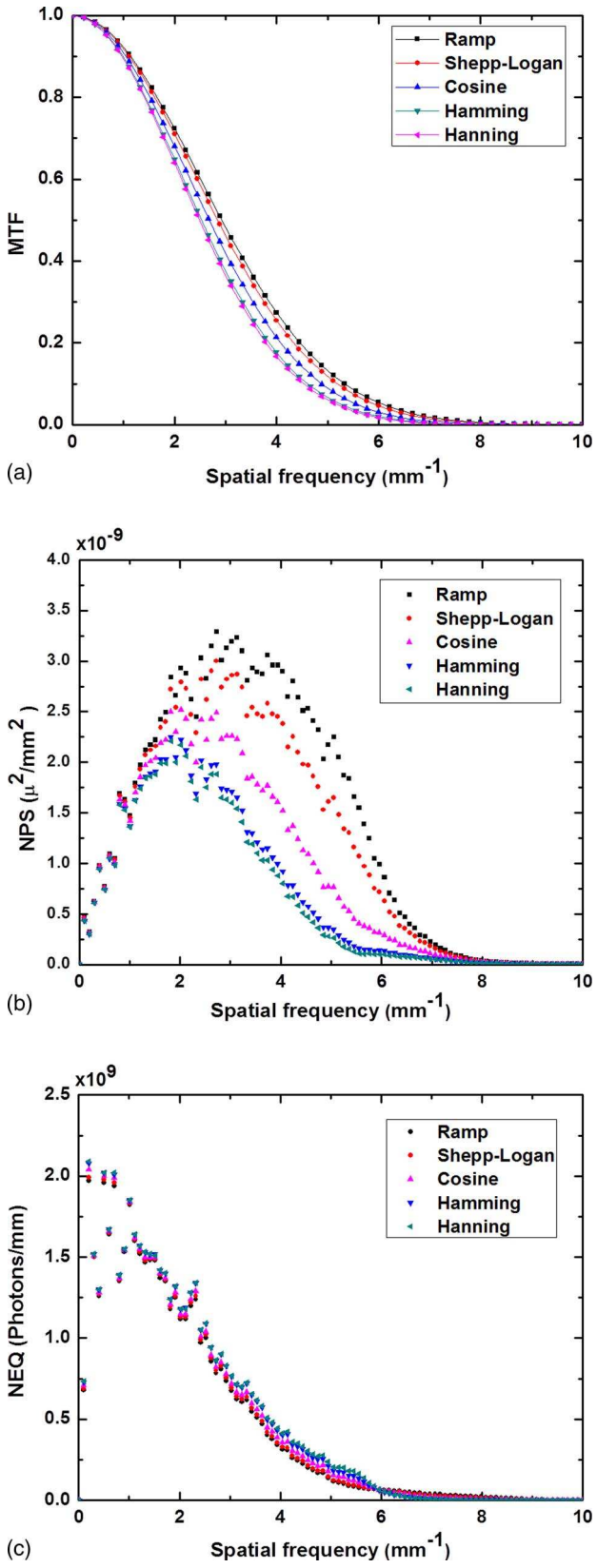

FIG. 9. (a) The axial MTF, (b) 2D NPS, and (c) 2D NEQ with a variety of reconstruction filters at 3 mGy.

fast ASIC readout and solid-state detector technology preserves the same energy resolution at higher fluxes. The photo peak from the characteristic $K\alpha$ x-rays for the Ag daughter product from the ^{109}Cd decay appears at 22 keV which verifies the energy calibration performed using a calibrated x-ray tube.

Generally, breast CT imaging techniques require a lower x-ray flux than other CT applications.[11] Furthermore, photon counting detectors can minimize dose using optimal energy weighting. However, spectral distortion correction is needed to generate an energy weighted image without artifacts.[32] The contribution of electronic noise becomes significant for energy-integrating detectors in low dose condition potentially producing poor quality images, whereas photon counting detectors may offer clinically acceptable image quality under the same dose conditions. The electronic noise level of the prototype Si-based photon counting detector, 4 keV, is lower than other previously reported photon counting detectors at 9.5,[33] 20,[34] or 22 keV.[11] Since lower energy photons usually produce more contrast, this Si-based photon counting detector can potentially provide significantly better low-contrast lesion detectability than other presently available photon counting detectors.

The prototype Si-based photon counting detector is pixelated with a pitch of 100 μm to offer a high in-plane resolution for detecting microcalcifications. The MTF results in Fig. 8(a) indicate that a 93 μm in diameter object can be distinguished under a magnification of 1.1. The noise dependence according to the doses was shown in the 2D axial NPS in Fig. 8(b) and the 2D axial NEQ in Fig. 8(c). The variation of NPS and NEQ, depending on dose, was more dominant at low spatial frequency than high spatial frequency. In terms of dose, a high dose will have high visibility of the lesions by reduced statistical noise. However, it is best to minimize the radiation dose for patients. The photon counting detector has a high potential for dose reduction in comparison to flat panel energy-integrating detectors when we use an optimal energy weighting method based on spectral information.[11] While a fine pixel pitch offers high spatial resolution, the increased statistical noise due to the lower number of counts per pixel in the image may reduce the visualization of low contrast lesions. A typical method for a compromise between statistical noise and spatial resolution is through the use of image reconstruction with various smoothing filters. When we increase the smoothing factor, the MTF and NPS decrease. Since the NEQ is calculated by the ratio of the MTF and NPS, the smoothing filters showed a very small effect on the NEQ [Fig. 5(c)]. We can expect the visibility of the lesion will be similar in terms of SNR even though we are using different reconstruction filters from the NEQ result. The effect of the data acquisition and reconstruction parameters will vary according to a task specification such as size and contrast even though there are small differences in physical characteristics.[35]

There are several factors which need to be considered in the design of a spectral breast CT system with the investigated Si strip detector. The first factor to consider is the increased quantum noise as a result of the 100 μm pixel pitch, which can result in reduced CNR in the acquired images. A low contrast target will be more susceptible to this factor, but this issue can be addressed by using a smoothing filter during the image reconstruction. However, a smoothing filter may

result in greater partial volume effect, which can potentially further reduce the contrast of microcalcifications. For this reason, we have proposed to use an imaging task-specific filter during the reconstruction. Sharp filters will be used for microcalcification detection in order to minimize the partial volume effect. A smoothing filter will be used for low-contrast lesions, which are less effected by the partial volume effect because of their large size. Another factor is that Compton scatter is a major source of performance degradation in Si.[36] However, due to the low tube voltage used in breast imaging, the Compton scattering cross section will remain relatively low and most of the Compton photons are expected to have a small scattering angle, which will lead to a small loss of its incident energy. Nevertheless, we have planned to use specific methods to address potential issues associated with Compton scattering. Compton electrons generally have energies below 15 keV, which can be rejected by setting the detector noise floor at 15 keV. We will also investigate the feasibility of anticoincidence logic in the ASICs by implementing the ability to reject counts that are recorded simultaneously in two pixels and only register the pixel with the largest signal.[37] The other factor is the tiling of multiple Si strip detectors to create a large enough FOV to create a fan beam geometry covering the breast. Although 0.6 mm of Si in the incident direction provides QDE of 67% at 60 kVp, depth of interaction (DOI) errors will limit the spatial resolution away from the center of the FOV if the detectors are mounted in a straight line. The detectors must, therefore, be tiled in a slight arc with each one pointed toward the x-ray focal spot. This along with a guard ring surrounding the Si strips will generate a gap between detectors of at least several hundred μm and although the gap could be filled by interpolation this would degrade the spatial resolution and could limit microcalcification detection. Nevertheless, we have planned to use specific methods to address potential issues associated with the gap between detectors. Methods to segment the collimators to produce an individual fan beam for each detector will be explored. We will also investigate the feasibility of using helical scanning to provide an optimal exposure and even sampling of the breast.

5. CONCLUSIONS

The characteristics of a prototype photon counting Si strip detector were investigated for spectral breast CT. The prototype photon counting Si strip detector shows high output count rate, excellent spatial and energy resolution, and low noise characteristics which are advantageous for breast CT imaging. Further studies are required to investigate correlation between specific task such as soft tissue lesion and microcalcifications detectability and characteristics of the spectral breast CT system according to the data acquisition and reconstruction parameters.

ACKNOWLEDGMENTS

This work was supported in part by NIH/NCI Grant No. R01CA13687.

[a]Author to whom correspondence should be addressed. Electronic mail: symolloi@uci.edu; Telephone: (949) 824-5904; Fax: (949) 824-8115.

[1]R. Siegel, D. Naishadham, and A. Jemal, "Cancer statistics, 2013," CA. Cancer J. Clin. **63**, 11–30 (2013).
[2]L. T. Niklason, B. T. Christian, L. E. Niklason, D. B. Kopans, D. E. Castleberry, B. Opsahl-Ong, C. E. Landberg, P. J. Slanetz, A. A. Giardino, and R. Moore, "Digital tomosynthesis in breast imaging," Radiology **205**, 399–406 (1997).
[3]G. Gennaro, A. Toledano, C. di Maggio, E. Baldan, E. Bezzon, M. La Grassa, L. Pescarini, I. Polico, A. Proietti, and A. Toffoli, "Digital breast tomosynthesis versus digital mammography: A clinical performance study," Eur. Radiol. **20**, 1545–1553 (2010).
[4]T. H. Helbich, "Contrast-enhanced magnetic resonance imaging of the breast," Eur. J. Radiol. **34**, 208–219 (2000).
[5]S. Brennan, L. Liberman, D. D. Dershaw, and E. Morris, "Breast MRI screening of women with a personal history of breast cancer," Am. J. Roentgenol. **195**, 510–516 (2010).
[6]Y. Hirooka, N. Aika, T. Ishisugi, M. Ohguri, C. Nagashima, S. Morishita, Y. Kato, and C. Fukuda, "Recent advances in ultrasound imaging of breast lesions," Yonago Acta Med. **52**, 115–120 (2009).
[7]L. Chen, C. K. Abbey, A. Nosratieh, K. K. Lindfors, and J. M. Boone, "Anatomical complexity in breast parenchyma and its implications for optimal breast imaging strategies," Med. Phys. **39**, 1435–1441 (2012).
[8]K. K. Lindfors, J. M. Boone, T. R. Nelson, K. Yang, A. L. Kwan, and D. F. Miller, "Dedicated breast CT: Initial clinical experience1," Radiology **246**, 725–733 (2008).
[9]J. M. Boone, T. R. Nelson, K. K. Lindfors, and J. A. Seibert, "Dedicated breast CT: Radiation dose and omage quality evaluation1," Radiology **221**, 657–667 (2001).
[10]C.-J. Lai, C. C. Shaw, L. Chen, M. C. Altunbas, X. Liu, T. Han, T. Wang, W. T. Yang, G. J. Whitman, and S.-J. Tu, "Visibility of microcalcification in cone beam breast CT: Effects of x-ray tube voltage and radiation dose," Med. Phys. **34**, 2995–3004 (2007).
[11]H. Q. Le, J. L. Ducote, and S. Molloi, "Radiation dose reduction using a CdZnTe-based computed tomography system: Comparison to flat-panel detectors," Med. Phys. **37**, 1225–1236 (2010).
[12]W. A. Kalender, M. Beister, J. M. Boone, D. Kolditz, S. V. Vollmar, and M. C. Weigel, "High-resolution spiral CT of the breast at very low dose: Concept and feasibility considerations," Eur. Radiol. **22**, 1–8 (2012).
[13]C. Xu, M. Danielsson, S. Karlsson, C. Svensson, and H. Bornefalk, "Preliminary evaluation of a silicon strip detector for photon-counting spectral CT," Nucl. Instrum. Methods, Phys. Res. A **677**, 45–51 (2012).
[14]E. Roessl and R. Proksa, "K-edge imaging in x-ray computed tomography using multi-bin photon counting detectors," Phys. Med. Biol. **52**, 4679–4696 (2007).
[15]J. Siewerdsen, L. Antonuk, Y. El-Mohri, J. Yorkston, W. Huang, J. Boudry, and I. Cunningham, "Empirical and theoretical investigation of the noise performance of indirect detection, active matrix flat-panel imagers (AMFPIs) for diagnostic radiology," Med. Phys. **24**, 71–89 (1997).
[16]P. M. Shikhaliev and S. G. Fritz, "Photon counting spectral CT versus conventional CT: Comparative evaluation for breast imaging application," Phys. Med. Biol. **56**, 1905–1930 (2011).
[17]H. Bornefalk, C. Xu, C. Svensson, and M. Danielsson, "Design considerations to overcome cross talk in a photon counting silicon strip detector for computed tomography," Nucl. Instrum. Methods, Phys. Res. A **621**, 371–378 (2010).
[18]H. Bornefalk and M. Danielsson, "Photon-counting spectral computed tomography using silicon strip detectors: A feasibility study," Phys. Med. Biol. **55**, 1999–2022 (2010).
[19]M. Weigel, S. V. Vollmar, and W. A. Kalender, "Spectral optimization for dedicated breast CT," Med. Phys. **38**, 114–124 (2011).
[20]K. Taguchi and J. S. Iwanczyk, "Vision 20/20: Single photon counting x-ray detectors in medical imaging," Med. Phys. **40**, 1–19 (2013).
[21]G. F. Knoll, *Radiation Detection and Measurement* (Wiley, 2010).
[22]D. J. Tward and J. H. Siewerdsen, "Noise aliasing and the 3D NEQ of flat-panel cone-beam CT: Effect of 2D/3D apertures and sampling," Med. Phys. **36**, 3830–3843 (2009).
[23]D. J. Tward and J. H. Siewerdsen, "Cascaded systems analysis of the 3D noise transfer characteristics of flat-panel cone-beam CT," Med. Phys. **35**, 5510–5529 (2008).

[24]A. L. Kwan, J. M. Boone, K. Yang, and S.-Y. Huang, "Evaluation of the spatial resolution characteristics of a cone-beam breast CT scanner," Med. Phys. **34**, 275–281 (2007).
[25]H. Cho, H. Kim, Y. Choi, S. Lee, H. Ryu, and Y. Lee, "The effects of photon flux on energy spectra and imaging characteristics in a photon-counting x-ray detector," Phys. Med. Biol. **58**, 4865–4879 (2013).
[26]J. T. Bushberg and J. M. Boone, *The Essential Physics of Medical Imaging* (Lippincott/Williams & Wilkins, 2011).
[27]I. S. Kyprianou, S. Rudin, D. R. Bednarek, and K. R. Hoffmann, "Generalizing the MTF and DQE to include x-ray scatter and focal spot unsharpness: Application to a new microangiographic system," Med. Phys. **32**, 613–626 (2005).
[28]J. T. Dobbins III, E. Samei, N. T. Ranger, and Y. Chen, "Intercomparison of methods for image quality characterization. II. Noise power spectrum," Med. Phys. **33**, 1466–1475 (2006).
[29]K. Yang, A. L. Kwan, S.-Y. Huang, N. J. Packard, and J. M. Boone, "Noise power properties of a cone-beam CT system for breast cancer detection," Med. Phys. **35**, 5317–5327 (2008).
[30]K. L. Boedeker, V. N. Cooper, and M. F. McNitt-Gray, "Application of the noise power spectrum in modern diagnostic MDCT: Part I. Measurement of noise power spectra and noise equivalent quanta," Phys. Med. Biol. **52**, 4027–4046 (2007).
[31]P. M. Shikhaliev, "Computed tomography with energy-resolved detection: a feasibility study," Phys. Med. Biol. **53**, 1475–1495 (2008).
[32]T. G. Schmidt, "CT energy weighting in the presence of scatter and limited energy resolution," Med. Phys. **37**, 1056–1067 (2010).
[33]J. S. Iwanczyk, E. Nygard, O. Meirav, J. Arenson, W. C. Barber, N. E. Hartsough, N. Malakhov, and J. C. Wessel, "Photon counting energy dispersive detector arrays for x-ray imaging," IEEE Trans. Nucl. Sci. **56**, 535–542 (2009).
[34]W. C. Barber, E. Nygard, J. S. Iwanczyk, M. Zhang, E. C. Frey, B. M. Tsui, J. C. Wessel, N. Malakhov, G. Wawrzyniak, and N. E. Hartsough, paper presented at the SPIE Medical Imaging (unpublished).
[35]J. Baek, A. R. Pineda, and N. J. Pelc, "To bin or not to bin? The effect of CT system limiting resolution on noise and detectability," Phys. Med. Biol. **58**, 1433–1446 (2013).
[36]S. Yun, J. Tanguay, H. K. Kim, and I. A. Cunningham, "Cascaded-systems analyses and the detective quantum efficiency of single-Z x-ray detectors including photoelectric, coherent and incoherent interactions," Med. Phys. **40**, 041916 (17pp.) (2013).
[37]R. Ballabriga, M. Campbell, E. Heijne, X. Llopart, and L. Tlustos, "The Medipix3 prototype, a pixel readout chip working in single photon counting mode with improved spectrometric performance," IEEE Trans. Nucl. Sci. **54**, 1824–1829 (2007).